Chemical Engineering Journal 380 (2020) 122486

Contents lists available at ScienceDirect

Chemical Engineering Journal

journal homepage: www.elsevier.com/locate/cej

Hierarchical NiMn-layered double hydroxides@CuO core-shell heterostructure in-situ generated on $Cu(OH)_2$ nanorod arrays for high performance supercapacitors

Aitang Zhang[a,1], Wen Zheng[a,1], Zhen Yuan[b,*], Jinmi Tian[a], Lijun Yue[a], Rongkun Zheng[b], Di Wei[b], Jingquan Liu[a,b,*]

[a] College of Materials Science and Engineering, Institute for Graphene Applied Technology Innovation, Collaborative Innovation Centre for Marine Biomass Fibers, Materials and Textiles of Shandong Province, Qingdao University, Qingdao 266071, China
[b] College of Materials Science and Engineering, Linyi University, Linyi 276400, Shandong, China

HIGHLIGHTS

- A hierarchical NiMn-LDH@CuO/CF core-shell heterostructure was successfully prepared.
- The hybrid comprises of vertical NiMn-LDHs shell and tops tangled CuO nanowires core.
- The NiMn-LDH@CuO/CF electrode exhibits high capacitance of 6077 mF cm^{-2} at 2 mA cm^{-2}.
- The blue LED indicator can be lit up eight minutes by three ASCs connected in series.

GRAPHICAL ABSTRACT

A hierarchical core-shell heterostructure comprised of vertical and intercrossing ultrathin NiMn-LDHs nanosheets shell and slightly curly and tops tangled CuO nanowires core shows promising electrochemical storage properties.

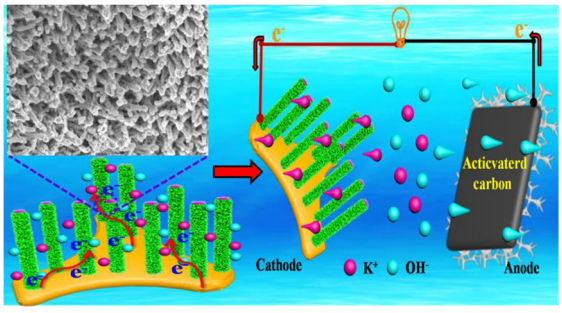

ARTICLE INFO

Keywords:
NiMn-LDH@CuO/CF
Core-shell hierarchical heterostructure
In situ growth
Nanowire arrays
Supercapacitor

ABSTRACT

Supercapacitors are attracting tremendous research interest because they are expected to achieve battery-level energy density while having long calendar life and short charging time. Ultrathin layered double hydroxide nanosheets (LDHs) are promising candidates as electrode materials for energy storage. Herein, we have successfully designed and synthesized a hierarchical NiMn-LDH@CuO/CF core-shell heterostructure which comprises a vertical and intercrossing ultrathin NiMn-LDHs nanosheets shell and a slightly curly and tops tangled CuO nanowires core. The synthesized NiMn-LDH@CuO/CF electrode exhibits a high areal capacitance of 6077 mF cm^{-2} (2430.8 F g^{-1}) at a current density of 2 mA cm^{-2} (0.8 A g^{-1}), which is significant higher than those of CF, $Cu(OH)_2$/CF, CuO/CF, NiMn-LDH/CF and NiMn-LDH electrodes. Moreover, a superior cycling stability of 89.22% retention after 8000 cycles at a high current density of 50 mA cm^{-2} is observed and a low internal resistance R_s (0.584 Ω) can be achieved. Furthermore, an all solid-state asymmetric supercapacitor (ASC) device based on the as-synthesized hierarchical NiMn-LDH@CuO/CF core-shell heterostructure hybrid material as positive electrode and activated carbon as negative electrode is successfully fabricated and exhibits

* Corresponding authors at: College of Materials Science and Engineering, Institute for Graphene Applied Technology Innovation, Collaborative Innovation Centre for Marine Biomass Fibers, Materials and Textiles of Shandong Province, Qingdao University, Qingdao 266071, China and College of Materials Science and Engineering, Linyi University, Linyi 276400, Shandong, China (J. Liu).
E-mail addresses: yuanzhen@lyu.edu.cn (Z. Yuan), jliu@qdu.edu.cn (J. Liu).
[1] Aitang Zhang and Wen Zheng contributed equally to this work.

https://doi.org/10.1016/j.cej.2019.122486
Received 11 June 2019; Received in revised form 27 July 2019; Accepted 11 August 2019
Available online 12 August 2019

an energy density of 10.8 W h kg^{-1} at a power density of 100 W kg^{-1}. Additionally, a LED indicator can be lit up for eight minutes when three ASCs are connected in series. The excellent electrochemical performances can be credited to the significant enhancement of the specific surface area, charge transport and mechanical stability resulted from the ultrathin LDH shell, the highly conductive CuO nanowires core-shell nanostructure. This strategy for the fabrication of hierarchical core-shell heterostructure could have enormous potential for applications in high performance energy storage devices.

1. Introduction

With the continually growing demand for clean energy and the rapid depletion of conventional fossil fuel, tremendous research efforts have been devoted to develop sustainable, high performance and environmentally friendly energy conversion and storage devices [1–5]. Particularly, the development of high-performance energy-storage devices as power sources is in urgent demand for the operation of electric vehicles, various electronic devices and other portable devices [6]. Electrochemical energy storage (EES), as an essential part of sustainable energy development, has attracted progressively scientific attention and become one of the key issues during the last few decades [7]. Among various emerging energy storage devices, electrochemical supercapacitors (SCs) have become one of the most competitive candidate for the next-generation electrochemical energy storage owing to their super high energy and power densities, superior rate capability, admirable safety and long cycling lifetime [8], which bridge the gap between traditional dielectric capacitors and chemical batteries [9–12]. Typically, SCs can be categorized into electrical double layer capacitors (EDLCs) and pseudocapacitors based on their charge storage mechanisms. For EDLCs, the charges were mainly adsorbed electrostatically at the electrode/electrolyte interface and many carbon-based materials like carbon nanotubes, activated carbons and graphene have been widely developed as electrode precursors on account of their huge specific surface area, superior conductivity and chemical stability [13]. However, pseudocapacitors store energy through the faradaic redox reactions based on redox active electrode materials, such as transition metal oxides and hydroxides [2,14]. In order to achieve a high performance of SCs, the electrode materials require to possess large specific areas, high conductivities, low fabrication costs, abundant resources and satisfactory electrochemical stability [15]. Many kinds of materials and material systems have been extensively investigated to improve the electrode performances, among which the redox-active transition metal oxides with unique nanostructures exhibited high specific capacitances owning to their good electrical conductivity, large surface area and highly reactive oxidation states [5,16].

Among multifarious transition metal oxides, ruthenium dioxide (RuO_2) has been employed as one of the most important electrode materials for supercapacitors due to its ultrahigh pseudocapacitance and reversibility of accepting and donating protons. However, the high cost and high toxicity severely restrict its actual commercial applications. Therefore, the development of low-cost metal oxides as alternatives is highly desirable [17,18]. Recently, copper oxide (CuO) with different nanostructures has attracted considerable attention among transition metal oxide nanostructures in the fields of supercapacitors due to its low cost, environmental friendliness, extensive sources, excellent chemical stability and desirable electrochemical properties [19–22]. Especially, when applied in pseudocapacitors, theoretical pseudocapacitance of CuO could reach up to 1800 F/g, which is close to that of the widely studied hydrated ruthenium oxide (~2200 F/g) [23]. Various novel CuO nanostructures have been intensively investigated for their electrochemical performance [24]. However, there are some serious limitations for single-phase metal oxides due to their low electrical conductivity and unstable cycling performances. Moreover, due to the drawbacks of individual electrode materials, single material electrode may not be able to meet the increasing demand of high energy density and long cycling stability, as well as fast charge-discharge rate. To overcome these drawbacks, one effective way is to incorporate other pseudocapacitive materials into copper oxides systems to enhance the electrical conductivity and consequently improve electrochemical properties, especially in the form of hierarchical core/shell nanowire arrays directly grown on three-dimensional (3D) conductive substrates [25,26]. Such hierarchical nanowire arrays can be directly employed as binder and conductive agent-free electrodes for high performance SCs [27]. Hybrid nanocomposites with different hierarchical structures and morphologies are employed [3]. Hence, many efforts have been focused on designing novel hierarchical structures to further improve their electrochemical performances [9].

Recently, layered double hydroxides (LDHs) as a class of emerging two-dimensional metal hydroxides have been intensely investigated as promising electrode materials for supercapacitors due to their intrinsic features of tunable chemical composition, good anion exchange behavior, high redox activity, inherent high stability and large surface area with exposed atoms [28–31]. However, the extensive applications are still restricted by their poor electronic conductivity and relatively slow ion transfer rates. In order to overcome these shortcomings [32], complex hydroxides/oxides of transition metals such as $NiO/Ni(OH)_2$ [33], $Ni(OH)_2@Mn_2O_3$ [34], $Co(OH)_2/Ni(OH)_2$ [35] and CoAl-LDH@$Ni(OH)_2$ [36] have been explored to achieve satisfactory faradaic capacitance owing to the richer redox reactions and higher electronic/ionic conductivities than their corresponding mono-component oxides or hydroxides [29]. Moreover, fundamental studies to improve pseudocapacitive performances using copper chalcogenide-based hybrid materials are still in the nascent stage and achieving the high capacitance and energy density for their practical application in supercapacitors is still in urgent demand [13].

In this work, a hierarchical NiMn-LDH@CuO/CF core-shell heterostructure which comprises of a vertical and intercrossing ultrathin NiMn-LDHs nanosheets shell and a slightly curly and tops tangled CuO nanowires core was synthesized and applied to fabricate a binder-free electrode which exhibited an excellent capacitive performance. The fabricated NiMn-LDH@CuO/CF electrode exhibited a high areal capacitance of 6077 mF cm^{-2} (2430.8 F g^{-1}) at a current density of 2 mA cm^{-2} (0.8 A g^{-1}) in a three electrodes system with 6 M KOH as the electrolyte, which is significant higher than that of CF, $Cu(OH)_2$/CF, CuO/CF, NiMn-LDH/CF and NiMn-LDH electrodes. Moreover, a superior cycling stability of 89.22% retention after 8000 cycles at a high current density of 50 mA cm^{-2} is observed and a low internal resistance R_s (0.584 Ω) can be achieved. Additionally, the as-synthesized hierarchical NiMn-LDH@CuO/CF core-shell heterostructure hybrid material can be utilized as the positive electrode to fabricate an all solid-state asymmetric supercapacitor device. The as fabricated NiMn-LDH@CuO/CF//AC ASC exhibited an energy density of 10.8 W h kg^{-1} at a power density of 100 W kg^{-1}. Additionally, a LED indicator can be lit up for eight minutes when three ASCs are connected in series. Therefore, the synthesized hierarchical NiMn-LDH@CuO/CF core-shell heterostructure has enormous potential for the fabrication of high performance energy storage devices.

2. Experimental sections

2.1. Materials

Copper foam and nickel foam were purchased from Shanghai

Zhongwei New Material Co., Ltd. Hydrochloric and ethanol (AR) were purchased from Tianjin Fuyu Fine Chemical Co., Ltd. Acetone, ethanol, sodium hydroxide (NaOH, AR), potassium hydroxide (KOH, AR), sodium thiosulfate pentahydrate ($Na_2S_2O_3{\cdot}5H_2O$, AR), ammonium persulfate ($(NH_4)_2S_2O_8$, AR), manganese (II) chloride tetrahydrate ($MnCl_2{\cdot}4H_2O$, AR), nickel(II) chloride hexahydrate ($NiCl_2{\cdot}6H_2O$, AR), hexamethylenetetramine (AR), acetylene black (AR), polyvinylidene fluoride (PVDF, AR) and activated carbon were all purchased from Sinopharm Chemical Reagent Co., Ltd. All aqueous solutions were prepared using deionized water with a resistivity of 18.2 MΩ·cm^{-1}. All of the chemicals were used as received without further purification.

2.2. In situ synthesis of $Cu(OH)_2$ nanorods on copper foam ($Cu(OH)_2$/CF)

Typically, the copper foam (1.0 × 1.0 cm^2) was ultrasonically cleaned with hydrochloric acid, acetone, ethanol and deionized water for 30 min individually to remove the surface oxide layer, respectively. After that, the copper foam was dried in vacuum oven under 50 °C adequately. Typically, 10.0 mL of 25 mmol NaOH aqueous solution and 10.0 mL of 1.25 mmol $(NH_4)_2S_2O_8$ aqueous solution were mixed under constant vigorously magnetic stirring to get a homogenous transparent solution. Subsequently, the pretreated copper foam was immersed into the above mixed solution for 10 min at ambient temperature. After the reaction, the light blue copper foam was taken out and washed with ethanol and deionized water for three times, respectively. Later, the resulting copper foam was desiccated in vacuum oven 50 °C to obtain the $Cu(OH)_2$/CF precursor.

2.3. Preparation of CuO nanowires on copper foam (CuO/CF)

CuO/CF was generated via a calcination process from the prepared $Cu(OH)_2$/CF precursor. In a typical procedure, the $Cu(OH)_2$/CF was calcined in a tube furnace and exposed to a flow of nitrogen atmosphere at 200 °C for 2 h at a heating rate of 5 °C/min to convert the $Cu(OH_2)$ by dehydration into CuO. After that, the brownish black CuO/CF nanoarrays were obtained.

2.4. Synthesis of hierarchical NiMn-LDH@CuO/CF core-shell heterostructures

The NiMn-LDHs coated CuO nanowires were synthesized through the hydrothermal strategy using CuO nanowires as template. In a typical procedure, 3 mmol of $NiCl_2{\cdot}6H_2O$, 1 mmol of $MnCl_2{\cdot}4H_2O$ and 5 mmol hexamethylenetetramine were dissolved in 30 mL deionized water and stirred for 30 min to form a homogenous solution. The obtained homogeneous solution was then transferred into a 50 mL Teflon-lined stainless steel autoclave. Subsequently, the prepared CuO/CF was immersed into the homogeneous solution and the autoclave was sealed for a hydrothermal reaction at 90 °C for 4 h before cooling to room temperature. Finally, the CuO/CF substrate supported NiMn-LDH was washed with deionized water for several times and dried at 60 °C in a vacuum drying oven. The corresponding mass loading of NiMn-LDHs on the CuO/CF substrate is found to be approximately 2.5 mg cm^{-2}.

2.5. Characterizations

The morphology of the as-synthesized products was analyzed by scanning electron microscope (SEM). SEM was operated at an accelerating voltage of 10 kV while EDX elemental mapping images were obtained on a JEOL JSM-6700F scanning electron microscope at an accelerating voltage of 20 kV. X-ray photoelectron spectroscopy (XPS) measurements were performed using a Kratos Axis Ultra DLD spectrometer employing a monochromated Al Ka X-ray source (h = 1486.7 eV). The crystallographic structures of the synthesized materials were determined by X-ray diffractometer with Cu-Kα radiation.

2.6. Fabrication of electrodes and electrochemical measurements

All the electrochemical measurements were performed on an electrochemical workstation (CHI 760E) (Shanghai Chenhua Instrument Factory, China) at ambient temperature. For the three-electrode tests, the synthesized samples of NiMn-LDH@CuO/CF (1.0 × 1.0 cm^2) were applied as the working electrodes directly while the platinum foil and the mercuric oxide electrode served as the counter and reference electrodes, respectively. 6 M KOH aqueous solution was used as the test electrolyte. Cyclic voltammetry (CV) tests were carried out in a potential range from 0.15 V to 0.54 V at diverse scan rates of 10, 20, 30, 40, 50, 60, 70, 80, 90 and 100 mV s^{-1}, respectively. Galvanostatic charge/discharge (GCD) curves were measured in a voltage range from 0.15 V to 0.54 V at different current densities of 2, 3, 5, 8, 10, 20, 30 and 50 mA cm^{-2}. Electrical impedance spectroscopy (EIS) measurements were performed in the frequency response range from 0.01 Hz to 100 kHz with a 5 mV AC perturbation at the open circuit potential. The specific capacitance of the electrodes can be calculated according to the GCD curves at different current densities using the following equation:

$$C_A = \frac{I \int V \Delta t}{sV^2} \tag{1}$$

where C_A (F cm^{-2}) is the areal capacitance, I_A is the discharge current, t (s) is the discharge time, V (V) is the potential window and s (cm^2) is the effective area of the electrode.

2.7. Preparation of KOH-based hydrogel electrolyte

Typically, 2 g of PVA was dispersed in 20 mL of deionized water at 80 °C to form a homogeneous solution. After the solution was cooled to about 65 °C, 10 mL of 6 M KOH solution was added with vigorous stirring to afford the KOH/PVA hydrogel electrolyte for further use.

2.8. Fabrication and electrochemical measurements of an all-solid state asymmetric supercapacitor (ASC)

To fabricate an active carbon (AC) electrode, active carbon, acetylene black, and polyvinylidene fluoride (PVDF) were mixed with ethanol in a mass ratio of 8:1:1 to obtain a slurry. Acetylene black and PVDF were used as a conductive agent and binder, respectively. Then the mixture was dried in a vacuum at 50 °C for 5 h. Afterwards, 10 mg of the resulting product was embedded into the nickel foam (1.0 × 1.0 cm^2). The ASC device was assembled by applying the as-prepared NiMn-LDH@CuO/CF (1.0 × 1.0 cm^2) as the positive electrode and AC as the negative one, respectively, while the pre-prepared KOH/PVA hydrogel served as the electrolyte. Typically, the as-prepared free-standing NiMn-LDH@CuO/CF and AC coated nickel foam electrodes were attached on copper films which worked as a current collector. Subsequently, the pre-prepared KOH/PVA gel electrolyte was dropped onto the surface of the NiMn-LDH@CuO/CF and AC coated nickel foam electrodes until saturation. Then the NiMn-LDH@CuO/CF and AC coated nickel foam electrodes were pressed together with little pressure which enabled the KOH/PVA gel electrolyte on each electrode to combine into one thin separating layer to achieve the NiMn-LDH@CuO/CF//AC ASC device. Here, PVA worked as both the solid gel electrolyte and a separator simultaneously. Compared to the supercapacitors packed with aqueous electrolytes and a separator, the polymer gel electrolyte of KOH/PVA exhibited excellent safety and stability. For obtaining an asymmetric supercapacitor with high electrochemical properties, the charge balance between the two electrodes should satisfy the relationship ($q^+ = q^-$), where q is the charge stored by the electrode, which can be calculated using the following equation [37]:

$$q = C \times m \times \Delta V \tag{2}$$

where C (F g^{-1}) is the specific capacitance of the electrode, m (g) is the

mass of the active material and V (V) is the potential window. According to the equation, the ideal mass ratio of electroactive material on the positive to that on negative electrode in an asymmetric supercapacitor (m^+/m^-) can be calculated using formula:

$$m^+/m^- = C^-\Delta V^-/C^+\Delta V^+ \quad (3)$$

where C^+ ($F\,g^{-1}$) and C^- ($F\,g^{-1}$) are the specific capacitances of the synthesized material and AC electrodes, respectively. V^+ (V) and V^- (V) are the voltage range of the synthesized sample and AC electrodes, respectively. The specific capacitance (Cs) of the ASC can be calculated from the galvanostatic charge-discharge curves according to the following equation:

$$C_S = \frac{I\int V\Delta t}{mV^2} \quad (4)$$

where I (A) is the discharge current, t (s) is the discharge time, V (V) is the potential window, and m (g) is the total mass of active materials on both electrodes. The energy density E ($W\,h\,kg^{-1}$) and power density P ($W\,kg^{-1}$) can be calculated according to equations as illustrated below:

$$E = \frac{1}{2}C_s\Delta V^2 \quad (5)$$

$$P = E/\Delta t \quad (6)$$

3. Results and discussions

The step-wise synthesis of hierarchical NiMn-LDH@CuO/CF core-shell heterostructure via in-situ wet oxidation and hydrothermal process is schematically illustrated in Fig. 1a. Briefly, Cu foam was applied as the substrate due to its 3D porous structure and excellent electronic conductivity. Nanorods were fully covered on the surface of Cu foam via a simple in situ wet oxidation process at room temperature. Subsequently, bunch-like CuO/CF nanowires with a slightly curly and tops tangled were derived through a facile calcination treatment of the Cu $(OH)_2$/CF nanorods precursor. After that, the NiMn-LDH nanosheets were grown uniformly on the CuO nanowires skeleton through the hydrothermal process, forming NiMn-LDH@CuO/CF core-shell heterostructure on Cu foam substrate. The as-synthesized hierarchical heterostructure with 3D grid structure and ultrathin LDH nanosheets provides a high specific surface area that can increase the number of active sites and promote the charge transfer and redox reactions during electrochemical applications.

The morphological and structural evolution of the step-wise

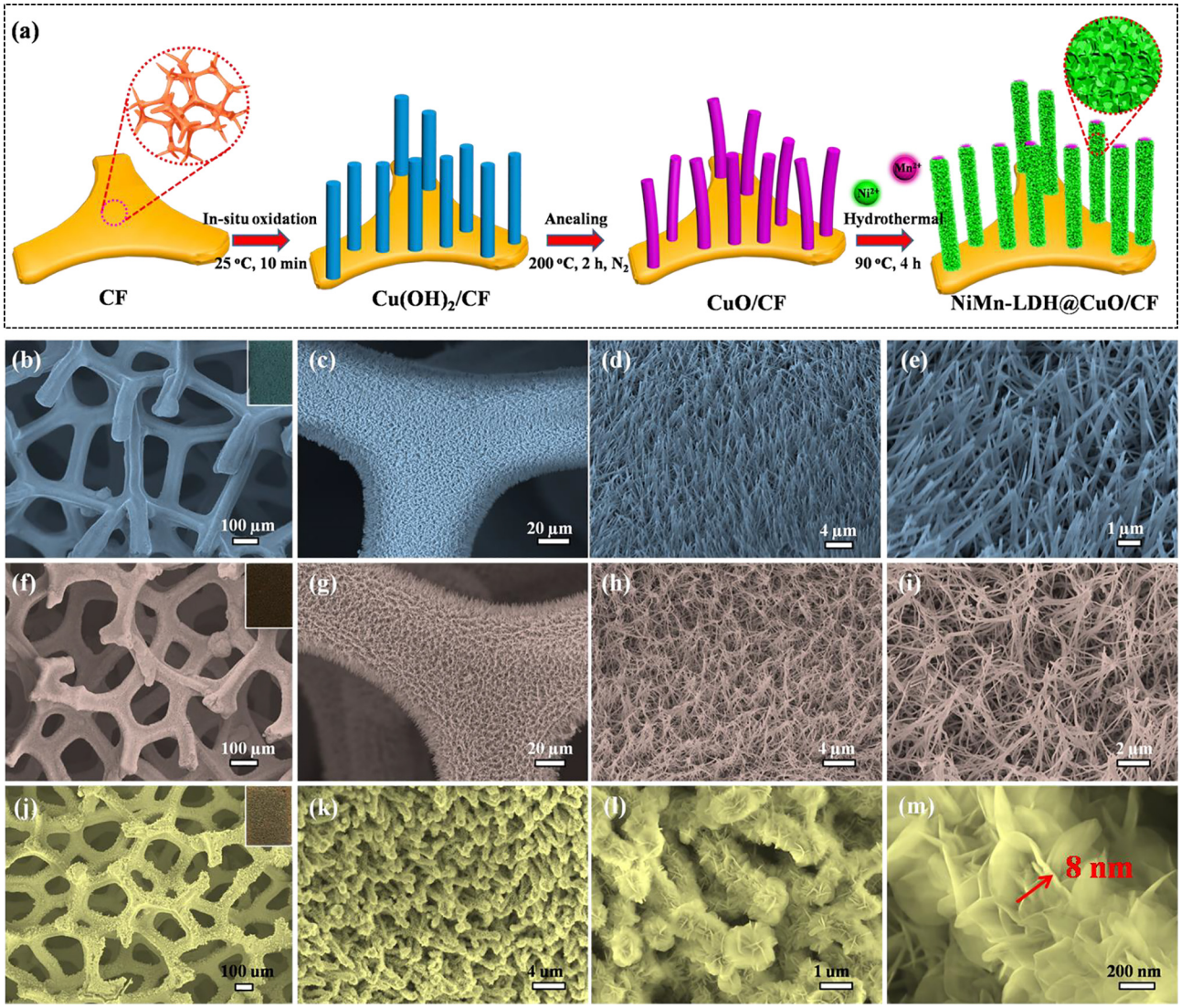

Fig. 1. (a) Schematic illustration for the step-wise preparation of hierarchical NiMn-LDH@CuO/CF core-shell heterostructure. (b–c) Low and (d–e) high magnification SEM images of the $Cu(OH)_2$/CF nanorod arrays. (f–g) Low and (h-i) high magnification SEM images of the CuO/CF nanowire arrays. (j–k) Low and (l–m) high magnification SEM images of the synthesized hierarchical NiMn-LDH@CuO/CF core-shell heterostructure.

synthesized materials were first investigated using scanning electron microscope (SEM). CuO/CF nanowires were synthesized through a facile calcination treatment of $Cu(OH)_2$/CF nanorods precursor which was obtained via a simple in situ wet oxidation process of Cu foam at room temperature. SEM image (Fig. S1) of the bare Cu foam shows that Cu foam has 3D porous structure with micrometer-sized pores, demonstrating that Cu foam can be utilized as a good template for surface modification. It can be seen from Fig. 1b–e, the utilized Cu foam was fully covered with crossed $Cu(OH)_2$ nanorods after the wet-oxidation process and the Cu foam still remained the 3D grid structure. After the calcination treatment, $Cu(OH)_2$ nanorods were converted into CuO nanowires, forming bunch-like nanowire arrays as shown in Fig. 1f–i. Interestingly, the reddish brown Cu foam was turned into light blue after oxidation and further changed to brownish black after calcination treatment at 200 °C as shown in the inset of Fig. 1f, indicating the corresponding phase transformations.

The NiMn-LDHs coated CuO nanowires were synthesized through a hydrothermal strategy and the resulting products exhibit the core-shell morphology as shown in Fig. 1j–m. Low magnification SEM images (Fig. 1j–k) shows the generated NiMn-LDHs uniformly covered on 3D grid support (Fig. 1m) which is fully covered with the slightly curly and tops tangled CuO nanowires. According to Fig. 1l–m images, the NiMn-LDH@CuO/CF hybrid heterostructures comprise of vertical and intercrossing ultrathin NiMn-LDHs nanosheets shell and a CuO nanowires core. The thickness of the NiMn-LDHs nanosheets is approximately 8 nm. The as-synthesized hybrid heterostructure, the slightly curly and tops tangled CuO nanowires and ultrathin NiMn-LDHs nanosheets are beneficial to enlarge the number of active sites and promote charge transfer rate as well as the redox reactions.

To better understand the chemical composition and detailed structures of the synthesized CuO/CF precursor and hierarchical NiMn-LDH@CuO/CF core-shell heterostructure, transmission electron microscope (TEM), high resolution transmission electron microscope (HRTEM), selected area electron diffraction (SAED), energy dispersive X-ray (EDX) and element mapping analyses were performed. As shown in Fig. 2a, the CuO nanowires exhibited smooth surface with average diameter of 50 nm. Additionally, Fig. 2b reveals well-ordered lattice planes with average spacings of 0.232 nm and 0.250 nm which can be attributed to the (1 1 1) and (1 1-1) lattice spacings of CuO, respectively. Fig. 2d shows the surface of CuO nanowires are fully covered with the ultra-thin NiMn-LDH nanosheets. Moreover, the HRTEM image depicted in Fig. 2e reveals the ordered lattice planes of NiMn-LDH nanosheets with average spacings of 0.231 nm and 0.260 nm which should be attributed to the (0.15) and (0.12) lattice spacings, respectively [38]. The SAED patterns shown in Fig. 2c and f all exhibit well-defined diffraction rings, indicating the polycrystalline nature of the obtained CuO/CF and NiMn-LDH@CuO/CF. Furthermore, the EDX spectrum shown in Fig. 2i and its corresponding element mapping images shown in Fig. 2h of NiMn-LDH@CuO/CF evidence the uniform distribution of Cu, O, Ni and Mn elements, which confirm the successful

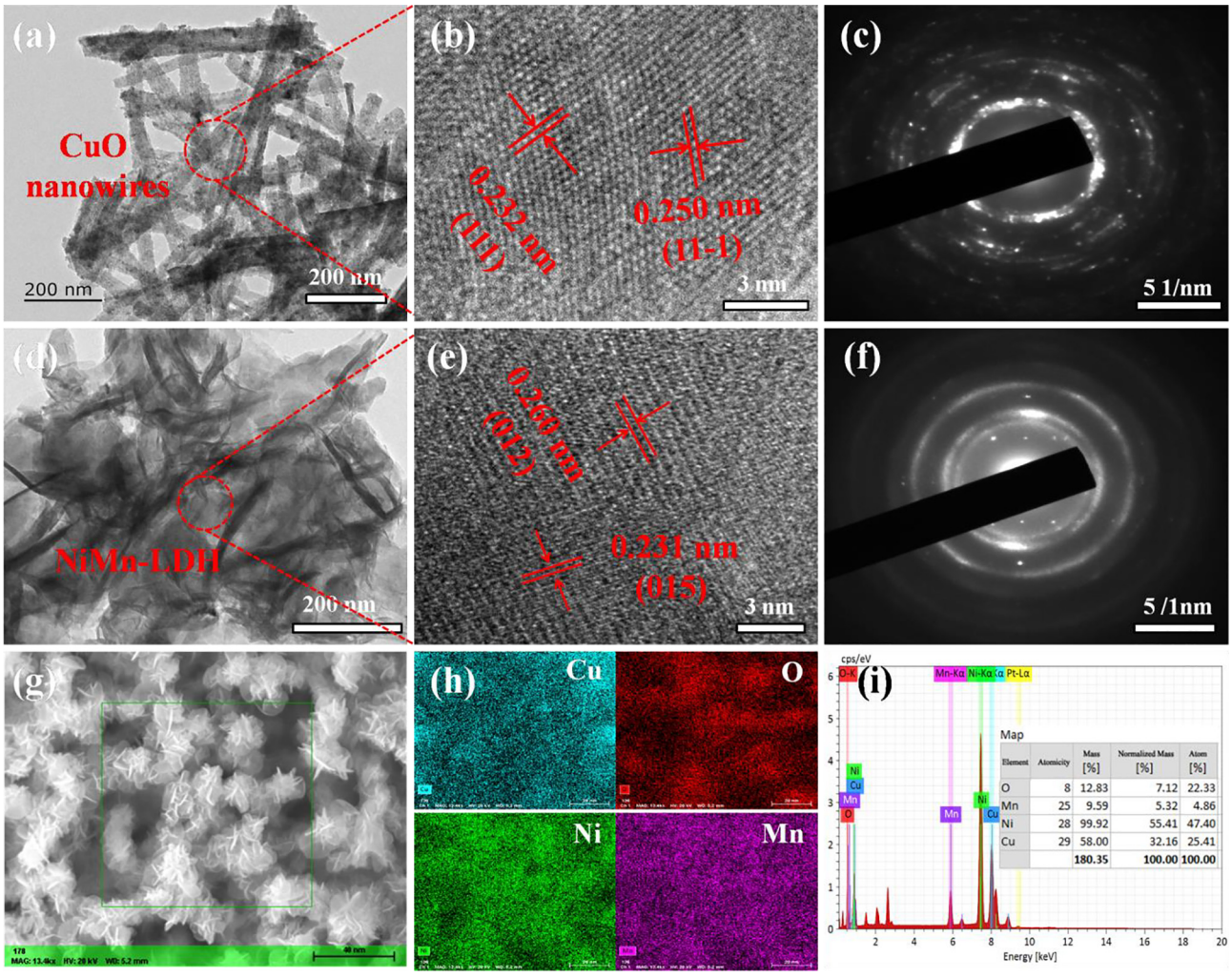

Fig. 2. (a) TEM, (b) HRTEM and the corresponding (c) SAED images of CuO/CF. (d) TEM, (e) HRTEM and its corresponding (f) SAED images of NiMn-LDH@CuO/CF. (g) SEM image and its (h) EDX elemental mapping images of NiMn-LDH@CuO/CF. (i) EDX spectrum of NiMn-LDH@CuO/CF.

synthesis of the hierarchical NiMn-LDH@CuO/CF core-shell heterostructure.

Additionally, X-ray photoelectron spectroscopy (XPS) is carried out to further investigate the different valence states of NiMn-LDH@CuO/CF and the results are shown in Fig. 3a–f. The full survey spectrum of the synthesized NiMn-LDH@CuO/CF shown in Fig. 3a confirms the coexistence of Cu, O, Ni and Mn elements. The high-resolution of Cu 2p, O 1s, Ni 2p and Mn 3s and Mn 2p spectra are shown in Fig. 3b-f. The Cu 2p spectrum shown in Fig. 3b can be deconvoluted into two peaks located at 932.5 eV (Cu $2p_{3/2}$) and 952.2 eV (Cu $2p_{1/2}$) with three strong satellite peaks located 940.9 eV, 943.7 eV and 962.2 eV [39]. Fig. 3c shows the O 1s spectrum which can be deconvoluted into three main peaks. The peaks located at 531.7 eV and 529.9 eV should be attributed to the oxygen atoms in CuO, while the peaks appeared at 530.7 eV should result from the oxygen atoms in $Cu(OH)_2$. The spectrum of Ni 2p is well fitted with two spin-orbit doublets and two shakeup satellites. Fig. 3d shows the peak of Ni $2p_{3/2}$ at 855.7 eV and the spin-orbit splitting value of Ni $2p_{1/2}$ and Ni $2p_{3/2}$ reaches 17.9 eV, indicating the main composition is Ni^{2+}. Moreover, the peaks at binding energies of 861.3 eV and 873.5 eV should be attributed to the satellite peaks of Ni $2p_{3/2}$ and Ni $2p_{1/2}$, respectively. The Mn 2p spectrum shown in Fig. 3f can be deconvoluted into two peaks appeared at 644.55 eV and 657.8 eV, which should be attributed to the characteristic peak of Mn $2p_{3/2}$ and Mn $2p_{1/2}$, respectively. Additionally, the Mn 3s spectrum can be deconvoluted into two characteristic peaks which located at 75.52 eV and 77.87 eV [40,41]. Moreover, the spectrum for C 1s shown in Fig. S2 can be deconvoluted into three peaks at 284.8 eV, 286 eV and 288.6 eV, which may be attributed to C−C/C=C, C−O and C=O originated from the air atmosphere, respectively. The results confirm that the synthesized NiMn-LDH@CuO/CF comprised of the cations Cu^{2+}, Ni^{2+} and Mn^{3+}. Additionally, the XPS results of NiMn-LDH@CuO/CF after the electrochemical tests are shown in Fig. S13. It is worthy to know that the chemical composition of the synthesized material plays an important role to achieve a high electrochemical performance.

XRD was then applied to characterize the crystallinity change from CF to NiMn-LDH@CuO/CF. As depicted in Fig. 3g, all the synthesized samples have the common three strong diffraction peaks at 43.4°, 50.6° and 74.3°, which should be ascribed to the metallic copper (JCPDS No. 04-0836) of CF substrates. The $Cu(OH)_2$/CF nanorods show diffraction peaks at 20.6°, 23.1°, 39.8° and 53.4°, which can be indexed to the orthorhombic phase of $Cu(OH)_2$ (JCPDS No. 35-0505), demonstrating the successful synthesis of $Cu(OH)_2$. After the calcination treatment, peaks for CuO (JCPDS No. 45-0937) were observed besides the peaks of bare CF, which clearly indicated the conversion of $Cu(OH)_2$ into CuO upon thermal treatment [42]. After generation of NiMn-LDH nanosheets on the surface of CuO nanowires, new diffraction peaks located at 11.330°, 22.568°, 35.745°, 59.837° and 61.193° were observed, which should be attributed to the (0 0 3), (0 0 6), (0 1 2), (1 1 0) and (1 1 3) planes of NiMn-LDHs, respectively [32]. Furthermore, the specific surface area of the NiMn-LDH@CuO/CF was then measured to be

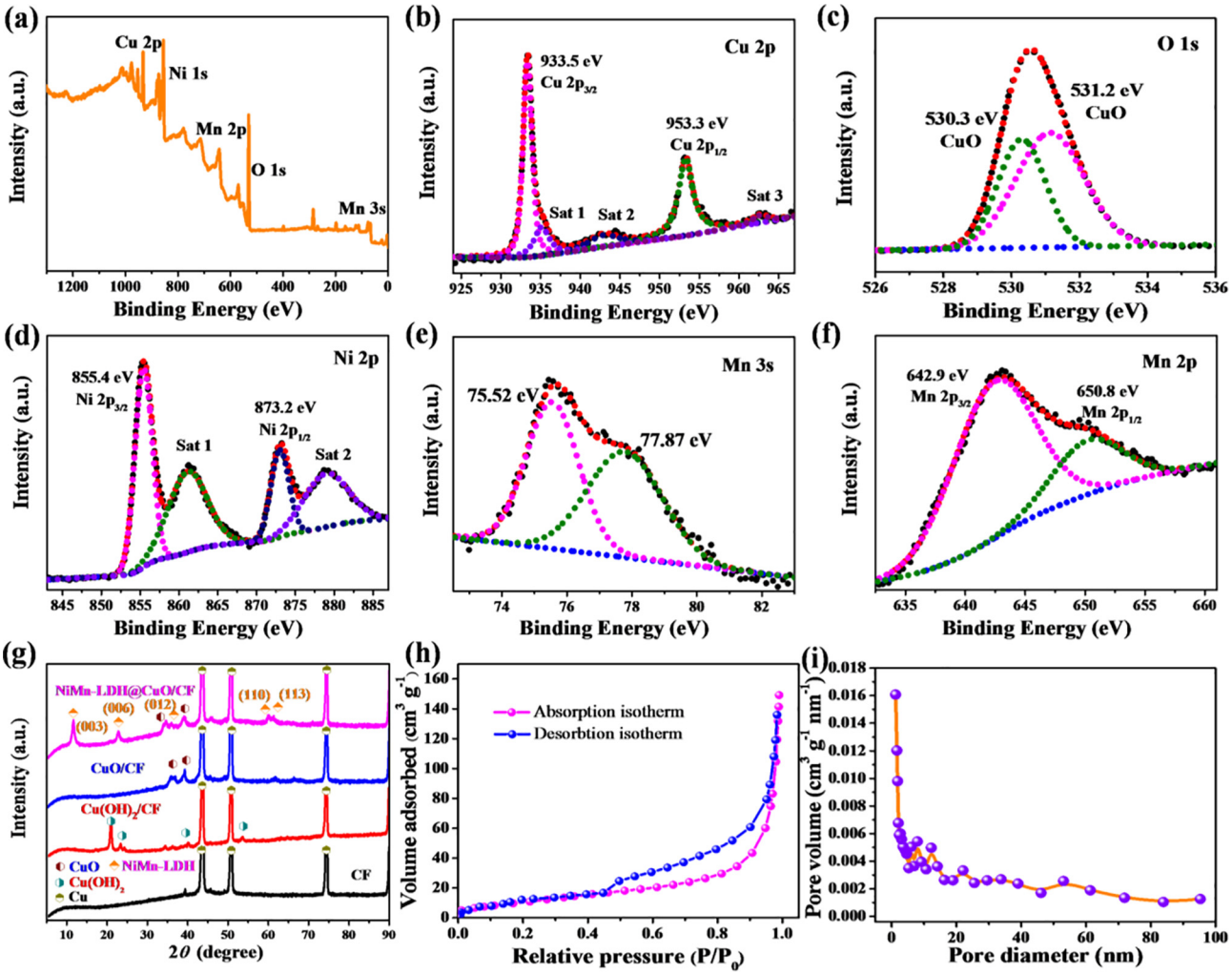

Fig. 3. (a) Survey XPS spectrum and high-resolution spectra for Cu 2p (b), O 1s (c), Ni 2p (d), Mn 3s (e) and Mn 2p (f) of the NiMn-LDH@CuO/CF. (g) The XRD pattern of the as-prepared samples. (h) The nitrogen adsorption-desorption isotherm of the NiMn-LDH@CuO/CF. (i) The pore-size distribution of the NiMn-LDH@CuO/CF.

41.772 m^2/g by Brunauer-Emmett-Teller (BET) and the N_2 adsorption-desorption isotherm is shown in Fig. 3h. Moreover, the mean pore diameter was measured to be 22.076 nm and the total pore volume was 0.2305 cm^3/g.

Electrochemical performances of the fabricated electrodes based on CF, $Cu(OH)_2$/CF, CuO/CF and NiMn-LDH@CuO/CF samples were all tested in a three-electrode system, applying a piece of Pt as the counter electrode and Hg/HgO as the reference electrode in 6 M KOH aqueous electrolyte. The cyclic voltammograms (CVs) of NiMn-LDH@CuO/CF electrode measured at different scan rates range from 10 to 100 mV s^{-1} in a potential window of 0.15–0.54 V are shown in Fig. 4c. The redox potentials of the fabricated NiMn-LDH@CuO/CF electrode were mainly located at 0.225 V and 0.46 V, respectively, as shown in Fig. 4c. As observed, the shape of CV curves exhibited significant redox peaks, indicating the capacitance of NiMn-LDH@CuO/CF electrode mainly derives from the faradaic redox reactions. Additionally, no obvious changes of the CV curve shapes are observed with the increasing scan rate, implying the excellent transport of electrons and ions. Moreover, it is apparent that the current intensity and the CV area of the NiMn-LDH@CuO/CF electrode are much larger than those of CF (Fig. S3), Cu $(OH)_2$/CF (Fig. S4), CuO/CF (Fig. S5), NiMn-LDH/CF (Fig. S10a) and NiMn-LDH (Fig. S10c) electrodes under the same scan rates, indicating the outstanding capacitive properties of the NiMn-LDH@CuO/CF electrode. Furthermore, the CVs of fabricated electrodes measured at a constant scan rate of 50 mV s^{-1} are shown in Fig. 4a and Fig. S10. As observed, the synthesized NiMn-LDH@CuO/CF electrode exhibits the largest CV curve area and redox peak intensity among all electrodes, which represents the highest specific capacitance and the fastest redox reaction kinetic process. The reversible redox reactions should be attributed to the valence transformation between Cu^{2+}/Cu^{+}, Ni^{+}/Ni^{2+} and Mn^{+}/Mn^{2+} couples, which can be illustrated by the following reactions [43–45]:

$$2CuO + H_2O + 2e^- \Leftrightarrow Cu_2O + 2OH^-$$

$$Cu_2O + H_2O + 2OH^- \Leftrightarrow 2Cu(OH)_2 + 2e^-$$

$$(CH_2)_6N_4 + 10H_2O \rightarrow 6HCHO + 4NH_4^+ + 4OH^-(1 - x)$$

$$Ni^{2+} + xMn^{2+} + 2OH^- \rightarrow (Ni_{1-x}Mn_x)(OH)_2$$

Moreover, as shown in Fig. 4d, the galvanostatic charge-discharge (GCD) curve shapes are nearly symmetric, demonstrating the high coulombic efficiency of the fabricated NiMn-LDH@CuO/CF electrode. Additionally, the discharge time of the prepared NiMn-LDH@CuO/CF electrode is much longer than those of other precursor electrodes at a

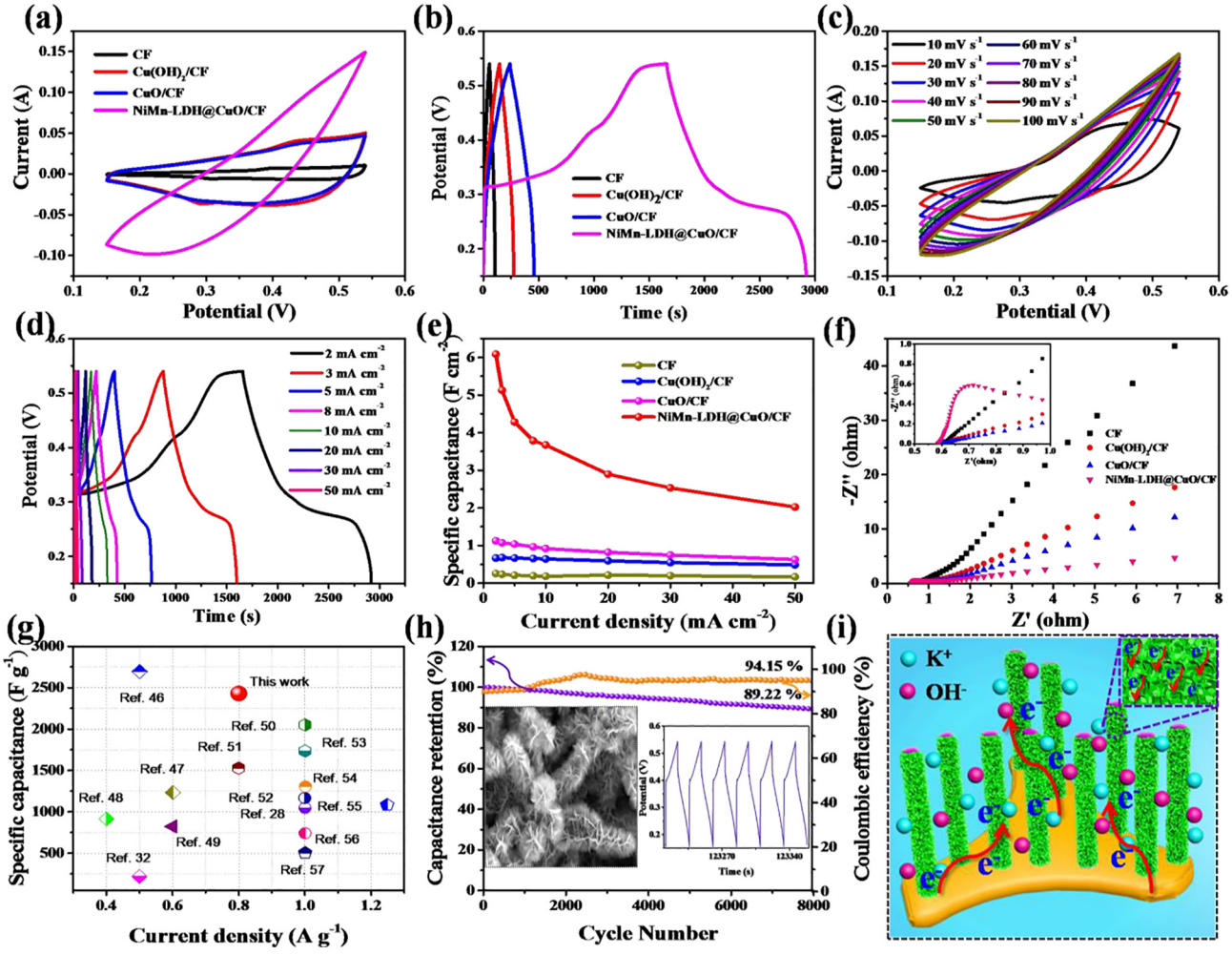

Fig. 4. Electrochemical performance measurements in three-electrode system. (a) CV curves of CF, $Cu(OH)_2$/CF, CuO/CF and NiMn-LDH@CuO/CF electrodes measured at the scan rate of 50 mV s^{-1}. (b) GCD curves of CF, $Cu(OH)_2$/CF, CuO/CF and NiMn-LDH@CuO/CF electrodes measured at the current density of 2 mA cm^{-2}. (c) CV and (d) GCD curves of NiMn-LDH@CuO/CF electrode tested at different scan rates and current densities, respectively. (e) The specific capacitance of the CF, $Cu(OH)_2$/CF, CuO/CF and NiMn-LDH@CuO/CF electrodes at different current densities. (f) Nyquist plots of CF, $Cu(OH)_2$/CF, CuO/CF and NiMn-LDH@CuO/CF electrodes. The inset shows the plots in high frequency range. (g) A comparison of specific capacitance with those reported by the literatures. (h) The cycling stability and coulombic efficiency of the NiMn-LDH@CuO/CF electrode at a current density of 50 mA cm^{-2}, the insets show the SEM image obtained after 8000st cycles and the last few CV cycles. (i) Schematic diagram interpreting why the NiMn-LDH@CuO/CF electrode has the enhanced electrochemical performances.

current density of 2 mA cm^{-2} as observed from Fig. 4b and Fig. S10. Furthermore, other precursor electrodes also exhibit a gradually decreased discharge time when the current density increasing range from 2 to 50 mA cm^{-2}, which indicates the remarkable reversibility during the charge-discharge process, agreeing with the CV curves. (Figs. S3–4 and S10) As observed, all fabricated electrodes exhibit similar CV and GCD curve shapes and tendency. Furthermore, the areal capacitances of all fabricated electrodes are calculated using the Eq. (1) based on the GCD curves. As shown in Fig. 4e, the areal capacitance of NiMn-LDH@CuO/CF electrode was measured to be approximately 6077 mF cm^{-2} (2372C cm^{-2}, as shown in Fig. S11) at a current density of 2 mA cm^{-2}, which is much higher than those of CF, Cu(OH)$_2$/CF, CuO/CF, NiMn-LDH/CF and NiMn-LDH electrodes. Additionally, the NiMn-LDH@CuO/CF electrode also shows remarkable rate capacity retention of approximately 89.22% of the initial capacitance.

Electrochemical impedance spectroscopy (EIS) was then applied to measure the internal resistances, charge transfer kinetics and ion diffusion processes of the fabricated electrodes. As shown in Fig. 4f, the curves for CF, Cu(OH)$_2$/CF, CuO/CF and NiMn-LDH@CuO/CF electrodes were derived from the sinusoidal signal in the frequency range from 0.01 Hz to 100 kHz with the amplitude of 5 mV. The internal resistance (R_s) derived from the intercept of the curve on the × axis at the high frequency is the sum of the intrinsic resistance of active materials, the electrolyte resistance and the contact resistance at the active material with the current collector interface. The R_s values of the CF, Cu(OH)$_2$/CF, CuO/CF and NiMn-LDH@CuO/CF electrodes were calculated to be 0.586 Ω, 0.594 Ω, 0.598 Ω and 0.584 Ω, respectively, indicating the NiMn-LDH@CuO/CF electrode had a relatively low intrinsic resistance and good conductivity. Additionally, the semicircle domain of the Nyquist plot in the middle frequency region should ascribe to the faradaic reactions and the diameter corresponds to the interfacial charge transfer resistance (R_{ct}). As observed, the NiMn-LDH@CuO/CF electrode has a comparatively small semicircle, demonstrating the lower R_{ct} and lower charge transfer resistance in the interface between electrode and electrolyte compared with other precursor electrodes. Moreover, the straight line in the low frequency region should be ascribed to Warburg impedance (Z_w) and the steep slope of the curves indicates the lower diffusion resistance and efficient ion diffusion between electrode and electrolyte during the redox reaction. The low impedance of NiMn-LDH@CuO/CF electrode also accounts for its excellent pseudocapacitive performance.

Additionally, the fabricated NiMn-LDH@CuO/CF electrode shows

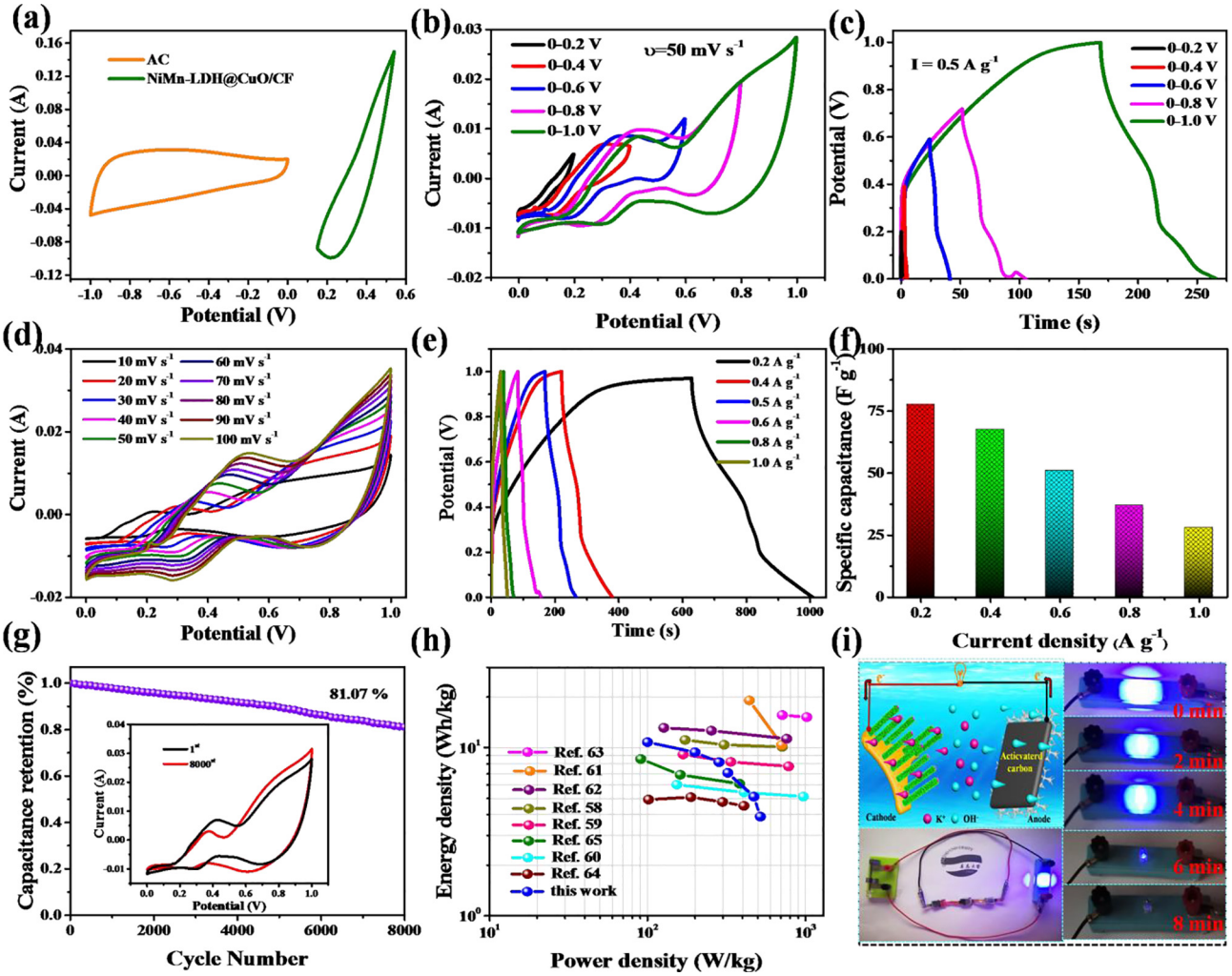

Fig. 5. Electrochemical characterization of the fabricated NiMn-LDH@CuO/CF//AC asymmetric all-solid state supercapacitor (ASC) device. (a) CV curves of AC and NiMn-LDH@CuO/CF electrodes tested in a three-electrode system in 6 M KOH electrolyte. (b) CV curves in different potential windows at a scan rate of 50 mV s^{-1}. (c) GCD curves in different potential windows at a current density of 0.5 A g^{-1}. (d) CV curves of the ASC at different scan rates in a potential window of 0–1 V. (e) GCD curves of the ASC at different current densities in a potential window of 0–1 V. (f) The specific capacitance of the ASC device measured at various current densities. (g) Cycling performance of the ASC measured at a current density of 5 A g^{-1} for 5000 cycles, the inset shows the CVs obtained at the 1st and 8000st cycles measured at 50 mV s^{-1}. (h) Ragone plot of the as-fabricated NiMn-LDH@CuO/CF//AC asymmetric supercapacitor device compared with the reported literatures. (i) LED indicator lit up by three solid-state ASCs connected in series and the brightness variation within eight minutes.

excellent specific capacitances of 2430.8F g^{-1} at the current density of 0.8 A g^{-1}, which is comparable or higher than most of electrodes fabricated based on the relative materials reported recently [28,32,46–57]. (Fig. 4g and Table S1) The excellent capacitance of NiMn-LDH@CuO/CF electrode may be attributed to the special design of the hierarchical heterostructure as shown in Fig. 4i. The in-situ synthesized CuO nanowires are directly distributed on the 3D grid Cu foam with the slight curly and tops tangled, which provide more paths for electrolyte shuttling. In addition, the CuO nanowires grown the precursor Cu foam with strong adhesion and therefore can be able to sustain mechanical integrity during the electrochemical process, resulting in prolonged cycling stability of the electrode. Moreover, the ultrathin NiMn-LDH nanosheets provide a large surface area and more abundant active sites for rapid intercalation of electrolyte ions, resulting in the enhanced electrochemical kinetics. The cycling stability of the NiMn-LDH@CuO/CF electrode was evaluated through galvanostatic charge-discharge measurement at the current density of 50 mA cm^{-2} and exhibited superior cycling stability of 89.22% retention after 8000 cycles as shown in Fig. 4h. Moreover, the coulombic efficiency was measured to be 94.15%. In addition, the shape of CVs obtained at the 8000st cycle is still similar to that at the 1st one under the scan rate of 100 mV s^{-1} as shown in Fig. S7, confirming the excellent cycling stability of the fabricated NiMn-LDH@CuO/CF electrode. Moreover, the SEM images of the NiMn-LDH@CuO/CF electrode after 8000 cycles revealed that the structure is well retained as shown in the inset of Fig. 4h, which further confirms the excellent stability and durability of the NiMn-LDH@CuO/CF electrode.

To further explore the practical application of the prepared electrode material in portable energy storage, an asymmetric all-solid state supercapacitor (ASC) device was fabricated using NiMn-LDH@CuO/CF as the positive electrode and AC coated nickel foam as the negative one. Fig. 5a shows the CV curves of AC and NiMn-LDH@CuO/CF electrodes, which were measured in a three-electrode system in 6 M KOH electrolyte. On the basis of the CV curves, both the AC and NiMn-LDH@CuO/CF electrodes make contribution to the overall capacitance of the fabricated ASC device. Fig. 5b and c show the CV and GCD curves of the NiMn-LDH@CuO/CF//AC ASC device tested at different potential windows at a scan rate of 50 mV s^{-1} and a current density of 0.5 A g^{-1}, respectively. The GCD curves also remain the similar shapes in different potential windows, indicating the considerable capacitive performance. The CV curves of the fabricated ASC device measured at different scan rates range from 10 to 100 mV s^{-1} in potential window of 0–1 V are shown in Fig. 5d. Additionally, the CV curves of the ASC device measured at different potential windows of 0–1.2 V and 0–1.6 V are shown in Fig. S9. The specific capacitance was calculated to be approximately 78 F g^{-1} at a current density of 0.2 A g^{-1} as shown in Fig. 5f. The Ragone plot related to energy and power densities at different current densities was also calculated based on the GCD curves. As shown in Fig. 5h, the fabricated device presents an energy density of 10.8 W h kg^{-1} at a power density of 100 W kg^{-1}, which is comparative with some of those previously reported [58–65]. Moreover, the specific capacitance retention can reach up to 81.07% even after 8000 cycles at 1 A g^{-1} compared with its initial capacitance as shown in Fig. 5g. Additionally, the schematic diagram of the NiMn-LDH@CuO/CF//AC ASC device fabricated using NiMn-LDH@CuO/CF as the cathode and AC as the anode is shown in the inset of Fig. 5i. Furthermore, a blue LED indicator (2.5 V) can be lit up for eight minutes by three solid-state ASCs connected in series as shown in Fig. 5i.

4. Conclusions

In summary, a hierarchical NiMn-LDH@CuO/CF core-shell heterostructure which comprises of a vertical and intercrossing ultrathin NiMn-LDHs nanosheets shell and a slightly curly and tops tangled CuO nanowires core was successfully synthesized and applied to fabricate a binder-free electrode which exhibited a high areal capacitance of 6077 mF cm^{-2} (2430.8 F g^{-1}) at a current density of 2 mA cm^{-2} (0.8 A g^{-1}), remarkable rate capacity of 1395 mF cm^{-2} at a current density of 50 mA cm^{-2} and excellent cycling stability of 89.22% retention after 8000 cycles. Furthermore, an all solid-state asymmetric supercapacitor was assembled with the as-synthesized hierarchical NiMn-LDH@CuO/CF core-shell heterostructure hybrid material which exhibits an energy density of 10.8 W h kg^{-1} at the power density of 100 W kg^{-1} and possesses the ability to light up a blue LED indicator for 8 min. The outstanding electrochemical performances can be credited to the significantly enhanced specific surface area, charge transport and mechanical stability by the ultrathin LDH shell, the highly conductive CuO nanowires core and the distinctive embedded core-shell nanostructure. Therefore, the as-synthesized hierarchical NiMn-LDH@CuO/CF core-shell heterostructure hybrid material has enormous potential for the fabrication of high performance energy storage devices for practical applications.

Declaration of Competing Interest

The authors declare no competing financial interest.

Acknowledgments

This work was supported by Qingdao Innovation Leading Talent Program, National Natural Science Foundation of China (21805124), and Natural Science Foundation of Shandong Province (ZR2018BEM020).

Appendix A. Supplementary data

Supplementary data to this article can be found online at https://doi.org/10.1016/j.cej.2019.122486.

References

[1] X. Cao, L. Cui, B. Liu, Y. Liu, D. Jia, W. Yang, et al., Reverse synthesis of star anise-like cobalt doped Cu-MOF/$Cu_{2+1}O$ hybrid materials based on $Cu(OH)_2$ precursor for high performance supercapacitors, J. Mater. Chem. A 7 (2019) 3815–3827.
[2] S. Kandula, K.R. Shrestha, N.H. Kim, J.H. Lee, Fabrication of a 3D hierarchical sandwich Co_9S_8 /α-MnS@N-C@Mo_S2 nanowire architectures as advanced electrode material for high performance hybrid supercapacitors, Small 23 (2018) 1800291.
[3] Y. Ouyang, X. Xia, H. Ye, L. Wang, X. Jiao, W. Lei, et al., Three-dimensional hierarchical structure ZnO@C@NiO on carbon cloth for asymmetric supercapacitor with enhanced cycle stability, ACS Appl. Mater. Interfaces 10 (2018) 3549–3561.
[4] L. Ying, X. Cao, D. Jiang, D. Jia, J. Liu, Hierarchical CuO nanorod arrays: in situ generated on three-dimensional copper foam via cyclic voltammetry oxidation for high-performance supercapacitors, J. Mater. Chem. A 6 (2018) 10474–10483.
[5] L. Yao, L. Li, C. Di, G. Shen, Nanowire-assembled Co_3O_4@$NiCo_2O_4$ architectures for high performance all-solid-state asymmetric supercapacitors, J. Mater. Chem. A 5 (2017) 24981–24988.
[6] G.S. Rama Raju, E. Pavitra, G. Nagaraju, S.C. Sekhar, S.M. Ghoreishian, C.H. Kwak, et al., Rational design of forest-like nickel sulfide hierarchical architectures with ultrahigh areal capacity as a binder-free cathode material for hybrid supercapacitors, J. Mater. Chem. A 6 (2018) 13178–13190.
[7] S. Liu, D. Ni, H.F. Li, S.C. Jun, K.N. Hui, C.Y. Ouyang, Effect of cation substitution on pseudocapacitive performance of spinel cobaltite MCo_2O_4 (M = Mn, Ni, Cu, and Co), J. Mater. Chem. A 6 (2018) 10674–10685.
[8] C. Qu, Z. Liang, Y. Jiao, B. Zhao, B. Zhu, D. Dang, et al., "One-for-all" strategy in fast energy storage: production of pillared MOF nanorod-templated positive/negative electrodes for the application of high-performance hybrid supercapacitor, Small 14 (2018) 1800285.
[9] H. Guan, C. Pan, X. Zhang, Y. Zhang, C. Gang, C. Dong, Cu_2O templating strategy for the synthesis of octahedral Cu_2O@$Mn(OH)_2$ core-shell hierarchical structures with superior performance supercapacitor, J. Mater. Chem. A 6 (2018) 13668–13675.
[10] Z. Sheng, Z. Wang, F. Huang, Z. Hui, S. Li, Hierarchical $Cu(OH)_2$@$Ni_2(OH)_2CO_3$ core/shell nanowire arrays in situ growth on three-dimensional copper foam for high-performance solid-state supercapacitors, J. Mater. Chem. A 5 (2017) 9960–9969.
[11] X. Cao, X. Wang, L. Cui, D. Jiang, Y. Zheng, J. Liu, Strongly coupled nickel boride/graphene hybrid as a novel electrode material for supercapacitors, Chem. Eng. J. 327 (2017) 1085–1092.
[12] Y. Zhao, S. Zhe, H. Li, C. Wang, Designing pinecone-like and hierarchical manganese cobalt sulfides for advanced supercapacitor electrode, J. Mater. Chem. A 6 (2018) 12782–12793.
[13] L. Ying, X. Cao, D. Jiang, D. Jia, J. Liu, Hierarchical cuo nanorod arrays in situ

generated on three-dimensional copper foam via cyclic voltammetry oxidization for high-performance supercapacitors, J. Mater. Chem. A 6 (2018) 10474–10483.
[14] D. Zhang, Y. Shao, X. Kong, M. Jiang, X. Lei, Hierarchical carbon-decorated Fe_3O_4 on hollow CuO nanotube array: fabrication and used as negative material for ultrahigh-energy density hybrid supercapacitor, Chem. Eng. J. 349 (2018) 491–499.
[15] Q. Chen, Y. Zhao, X. Huang, N. Chen, L. Qu, Three-dimensional graphitic carbon nitride functionalized graphene-based high-performance supercapacitors, J. Mater. Chem. A 3 (2015) 6761–6766.
[16] S.K. Shinde, V.J. Fulari, D.Y. Kim, N.C. Maile, R.R. Koli, H.D. Dhaygude, et al., Chemical synthesis of flower-like hybrid $Cu(OH)_2$/CuO electrode: application of polyvinyl alcohol and triton X-100 to enhance supercapacitor performance, Colloids Surf. B Biointerfaces 156 (2017) 165–174.
[17] T. Zhai, F. Wang, M. Yu, S. Xie, C. Liang, C. Li, et al., 3D MnO_2-graphene composites with large areal capacitance for high-performance asymmetric supercapacitors, Nanoscale 5 (2013) 6790–6796.
[18] R.R. Bi, X.L. Wu, F.F. Cao, L.Y. Jiang, Y.G. Guo, L.J. Wan, Highly dispersed RuO_2 nanoparticles on carbon nanotubes: facile synthesis and enhanced supercapacitance performance, J. Phys. Chem. C 114 (2010) 2448–2451.
[19] Y. Zhang, W.W. Guo, T.X. Zheng, Y.X. Zhang, X. Fan, Engineering hierarchical diatom@CuO@MnO_2 hybrid for high performance supercapacitor, Appl. Surf. Sci. 427 (2018) 1158–1165.
[20] I.Y.Y. Bu, R. Huang, Fabrication of CuO-decorated reduced graphene oxide nanosheets for supercapacitor applications, Ceram. Int. 43 (2017) 45–50.
[21] S.E. Moosavifard, M.F. El-Kady, M.S. Rahmanifar, R.B. Kaner, M.F. Mousavi, Designing 3D highly ordered nanoporous cuo electrodes for high-performance asymmetric supercapacitors, ACS Appl. Mater. Interfaces 7 (2015) 4851–4860.
[22] H. Kim, Y.K. Sang, J.L. Lun, A.E. Reddy, C.V.V.M. Gopi, Facile one-step synthesis of composite CuO/Co_3O_4 electrode material on ni foam for flexible supercapacitor applications, New J. Chem. 41 (2017) 5493–5497.
[23] B. Vidhyadharan, I.I. Misnon, R.A. Aziz, K.P. Padmasree, M.M. Yusoff, R. Jose, Superior supercapacitive performance in electrospun copper oxide nanowire electrodes, J. Mater. Chem. A 2 (2014) 6578–6588.
[24] T. Zhao, W. Yang, X. Ji, W. Jin, J. Hu, T. Li, In-situ synthesis of expanded graphite embedded with CuO nanospheres coated with carbon for supercapacitors, Appl. Surf. Sci. 460 (2018) 58–64.
[25] L. Zhou, Y. He, C. Jia, V. Pavlinek, P. Saha, Q. Cheng, Construction of hierarchical CuO/Cu_2O@$NiCo_2S_4$ nanowire arrays on copper foam for high performance supercapacitor electrodes, Nanomaterials (Basel) 7 (2017) 273.
[26] J. Lin, P. Wang, H. Wang, C. Li, X. Si, J. Qi, J. Cao, Z. Zhong, W. Fei, J. Feng, Defect-rich heterogeneous MoS_2/NiS_2 nanosheets electrocatalysts for efficient overall water splitting, Adv. Sci. 6 (2019) 1900246.
[27] Z. Sheng, Z. Wang, F. Huang, Z. Hui, S. Li, Hierarchical $Cu(OH)_2$@$Ni_2(OH)_2CO_3$ core/shell nanowire arrays in situ grown on three-dimensional copper foam for high-performance solid-state supercapacitors, J. Mater. Chem. A 5 (2017) 9960–9969.
[28] H. Tian, W. Bao, Y. Jiang, L. Wang, L. Zhang, O. Sha, et al., Fabrication of Ni-Al LDH/nitramine-N-doped graphene hybrid composites via a novel self-assembly process for hybrid supercapacitors, Chem. Eng. J. 354 (2018) 1132–1140.
[29] S. Liu, C.L. Su, U. Patil, I. Shackery, S. Kang, Z. Kan, et al., Hierarchical MnCo-layered double hydroxides@$Ni(OH)_2$ core-shell heterostructures as advanced electrodes for supercapacitors, J. Mater. Chem. A 6 (2017) 1043–1049.
[30] J. Lin, Y. Yan, X. Zheng, Z. Zhong, Y. Wang, J. Qi, J. Cao, W. Fei, Y. Huang, J. Feng, Designing and constructing core-shell $NiCo_2S_4$@Ni_3S_2 on Ni foam by facile one-step strategy as advanced battery-type electrodes for supercapattery, J. Colloid Interface Sci. 536 (2019) 456–462.
[31] X. Zhou, X. Li, D. Chen, D. Zhao, X. Huang, Ultrathin CoFe-layered double hydroxide nanosheets embedded in high conductance Cu_3N nanowire arrays with 3D core-shell architecture for ultrahigh capacitance supercapacitor, J. Mater. Chem. A 6 (2018) 24603–24613.
[32] D. Chen, S. Yan, H. Chen, L. Yao, W. Wei, H. Lin, et al., Hierarchical Ni-Mn layered double hydroxide grown on nitrogen-doped carbon foams as high-performance supercapacitor electrode, Electrochim. Acta 292 (2018) 374–382.
[33] X. Dai, D. Chen, H. Fan, Y. Zhong, L. Chang, H. Shao, et al., $Ni(OH)_2$/NiO/Ni composite nanotube arrays for high-performance supercapacitors, Electrochim. Acta 154 (2015) 128–135.
[34] K.S. Pei, R. Wang, Y. Ma, W. Hui, S. Yin, Ranunculus flower-like $Ni(OH)_2$@Mn_2O_3 as a high specific capacitance cathode material for alkaline supercapacitors, J. Mater. Chem. A 4 (2016) 7591–7595.
[35] J. Li, M. Yang, J. Wei, Z. Zhou, Preparation and electrochemical performances of doughnut-like $Ni(OH)_2$-$Co(OH)_2$ composites as pseudocapacitor materials, Nanoscale 4 (2012) 4498–4503.
[36] W. Hong, J.Q. Wang, L.Y. Niu, J.F. Sun, P.W. Gong, S.R. Yang, Controllable synthesis of CoAl LDH@$Ni(OH)_2$ nanosheet arrays as binder-free electrode for supercapacitor applications, J. Alloys Compd. 608 (2014) 297–303.
[37] M.S. Tamboli, D.P. Dubal, S.S. Patil, A.F. Shaikh, V.G. Deonikar, M.V. Kulkarni, et al., Mimics of microstructures of ni substituted $Mn_{1-x}Ni_xCo_2O_4$ for high energy density asymmetric capacitors, Chem. Eng. J. 307 (2017) 300–310.
[38] W. Guo, C. Yu, S. Li, J. Yang, Z. Liu, C. Zhao, et al., High-stacking-density, superior-roughness ldh bridged with vertically aligned graphene for high-performance asymmetric supercapacitors, Small 13 (2017) 170128.
[39] D. Ranjith Kumar, D. Manoj, J. Santhanalakshmi, Optimization of site specific adsorption of oleylamine capped CuO nanoparticles on mwcnts for electrochemical determination of guanosine, Sens. Actuators, B 188 (2013) 603–612.
[40] J. Lin, H. Jia, H. Liang, S. Chen, Y. Cai, J. Qi, et al., Hierarchical $CuCo_2S_4$@NiMn-layered double hydroxide core-shell hybrid arrays as electrodes for supercapacitors, Chem. Eng. J. 336 (2018) 562–569.
[41] H. Wan, J. Liu, Y. Ruan, L. Lv, L. Peng, X. Ji, et al., Hierarchical configuration of $NiCo_2S_4$ nanotube@Ni-Mn layered double hydroxide arrays/three-dimensional graphene sponge as electrode materials for high-capacitance supercapacitors, ACS Appl. Mater. Interfaces 7 (2015) 15840–110847.
[42] H. Chen, M. Zhou, T. Wang, F. Li, Y.X. Zhang, Construction of unique cupric oxide-manganese dioxide core-shell arrays on a copper grid for high-performance supercapacitors, J. Mater. Chem. A 4 (2016) 10786–10793.
[43] Y. Zhou, X. Zou, Z. Zhao, B. Xiang, Y. Zhang, CoO/RGO composite prepared by a facile direct-flame approach for high-power supercapacitors, Ceram. Int. 44 (2018) 16900–16907.
[44] X. Zhang, C. Zhang, A. Abas, Y. Zhang, X. Mu, J. Zhou, et al., Ag nanoparticles enhanced vertically-aligned CuO nanowire arrays grown on Cu foam for stable hybrid supercapacitors with high energy density, Electrochim. Acta 296 (2018) 535–544.
[45] J.H. Kim, D. Bhattacharjya, J.S. Yu, Synthesis of hollow TiO_2@N-doped carbon with enhanced electrochemical capacitance by an in situ hydrothermal process using hexamethylenetetramine, J. Mater. Chem. A 2 (2014) 11472–11479.
[46] J.-J. Zhou, Q. Li, C. Chen, Y.-L. Li, K. Tao, L. Han, Co_3O_4@CoNi-LDH core/shell nanosheet arrays for high-performance battery-type supercapacitors, Chem. Eng. J. 350 (2018) 551–558.
[47] M. Li, Y. Wang, H. Yang, P.K. Chu, Hierarchical $CoMoO_4$@Co_3O_4 nanocomposites on an ordered macro-porous electrode plate as a multi-dimensional electrode in high-performance supercapacitors, J. Mater. Chem. A 5 (2017) 17312–17324.
[48] S.P. Adhikari, G.P. Awasthi, K.S. Kim, C.H. Park, C.S. Kim, Synthesis of three-dimensional mesoporous Cu-Al layered double hydroxide/g-C_3N_4 nanocomposites on Ni-foam for enhanced supercapacitors with excellent long-term cycling stability, Dalton Trans. 47 (2018) 4455–4466.
[49] Q. Gui, J. Jiang, Y. Li, J. Liu, One-pot growth of $Co(OH)_2$ nanowire bundle arrays on in situ functionalized carbon cloth for robust flexible supercapacitor electrodes, Dalton Trans. 47 (2018) 15416–15423.
[50] X. Zheng, X. Han, X. Zhao, J. Qi, Q. Ma, K. Tao, et al., Construction of Ni-Co-Mn layered double hydroxide nanoflakes assembled hollow nanocages from bimetallic imidazolate frameworks for supercapacitors, Mater. Res. Bull. 106 (2018) 243–249.
[51] W. Zheng, S. Sun, Y. Xu, R. Yu, H. Li, Facile synthesis of NiAl-LDH/MnO_2 and NiFe-LDH/MnO_2 composites for high-performance asymmetric supercapacitors, J. Alloys Compd. 768 (2018) 240–248.
[52] X. Li, Z. Yang, W. Qi, Y. Li, Y. Wu, S. Zhou, et al., Binder-free Co_3O_4@nicoal-layered double hydroxide core-shell hybrid architectural nanowire arrays with enhanced electrochemical performance, Appl. Surf. Sci. 363 (2016) 381–388.
[53] D. Kong, J. Luo, Y. Wang, W. Ren, T. Yu, Y. Luo, et al., Three-dimensional Co_3O_4@MnO_2 hierarchical nanoneedle arrays: morphology control and electrochemical energy storage, Adv. Fun. Mater. 24 (2014) 3815–3826.
[54] S. Liu, D. Ni, H.F. Li, K.N. Hui, C.Y. Ouyang, S.C. Jun, Effect of cation substitution on the pseudocapacitive performance of spinel cobaltite MCo_2O_4(M = Mn, Ni, Cu, and Co), J. Mater. Chem. A 6 (2018) 10674–10685.
[55] H. Jia, Z. Wang, X. Zheng, J. Lin, H. Liang, Y. Cai, et al., Interlaced Ni-Co LDH nanosheets wrapped Co_9S_8 nanotube with hierarchical structure toward high performance supercapacitors, Chem. Eng. J. 351 (2018) 348–355.
[56] J. Xu, Y. Wang, S. Cao, J. Zhang, G. Zhang, H. Xue, et al., Ultrathin Cu-MOF@δ-MnO_2 nanosheets for aqueous electrolyte-based high-voltage electrochemical capacitors, J. Mater. Chem. A 6 (2018) 17329–17336.
[57] A.M. Zardkhoshoui, S.S.H. Davarani, Flexible asymmetric supercapacitors based on CuO@MnO_2-RGO and MoS_2-RGO with ultrahigh energy density, J. Electroanal. Chem. 827 (2018) 221–229.
[58] M. Kuang, T.T. Li, H. Chen, S.M. Zhang, L.L. Zhang, Y.X. Zhang, Hierarchical Cu_2O/CuO/Co_3O_4 core-shell nanowires: synthesis and electrochemical properties, Nanotechnology 26 (2015) 304002.
[59] M. Kuang, Z.Q. Wen, X.L. Guo, S.M. Zhang, Y.X. Zhang, Engineering firecracker-like beta-manganese dioxides@spinel nickel cobaltates nanostructures for high-performance supercapacitors, J. Power Sources 270 (2014) 426–433.
[60] Y. Wang, X. Zhang, X. Li, Y. Zhao, H. Wei, Y. Liu, et al., Highly dispersed ultrasmall $Ni(OH)_2$ aggregated particles on a conductive support as a supercapacitor electrode with superior performance, J. Colloid Interface Sci. 490 (2017) 252–258.
[61] J. Huang, P. Xu, D. Cao, X. Zhou, S. Yang, Y. Li, et al., Asymmetric supercapacitors based on β-$Ni(OH)_2$ nanosheets and activated carbon with high energy density, J. Power Sources 246 (2014) 371–376.
[62] C. Yuan, L. Zhang, L. Hou, G. Pang, W.-C. Oh, One-step hydrothermal fabrication of strongly coupled Co_3O_4 nanosheets-reduced graphene oxide for electrochemical capacitors, RSC Adv. 4 (2014) 14408–14413.
[63] X.F. Lu, D.J. Wu, R.Z. Li, Q. Li, S.H. Ye, Y.X. Tong, et al., Hierarchical $NiCo_2O_4$ nanosheets@hollow microrod arrays for high-performance asymmetric supercapacitors, J. Mater. Chem. A 2 (2014) 4706–4713.
[64] H. Yongmin, C. Wanjun, L. Xiaodong, Z. Zhenxing, F. Jiecai, Z. Changhui, et al., Freestanding three-dimensional graphene/MnO_2 composite networks as ultralight and flexible supercapacitor electrodes, ACS Nano 7 (2013) 174–182.
[65] Z. Lei, J. Zhang, X.S. Zhao, Ultrathin MnO_2 nanofibers grown on graphitic carbon spheres as high-performance asymmetric supercapacitor electrodes, J. Mater. Chem. 22 (2012) 153–160.